

DISCOVERY OF A T DWARF BINARY WITH THE LARGEST KNOWN J-BAND FLUX REVERSAL¹

Dagny L. Looper², Christopher R. Gelino³, Adam J. Burgasser⁴, J. Davy Kirkpatrick⁵

Submitted to ApJ on 29 February 2008; accepted on 19 May 2008; published on 1 October 2008

ABSTRACT

We present Keck laser guide star observations of two T2.5 dwarfs { 2MASS J11061197+ 2754225 and 2MASS J14044941 3159329 } using NIRC2 on Keck-II and find 2MASS J14044941 3159329 to be a 0^h13 binary. This system has a secondary that is 0.45 mags brighter than the primary in J-band but 0.49 mags fainter in H-band and 1.13 mags fainter in K_s-band. We use this relative photometry along with near-infrared synthetic modelling performed on the integrated light spectrum to derive component types of T1.5 for the primary and T5.5 for the secondary. Optical spectroscopy of this system obtained with Magellan/LDSS-3 is also presented. This is the fourth L/T transition binary to show a flux reversal in the 1.2 μm regime and this one has the largest flux reversal. Unless the secondary is itself an unresolved binary, the J-band magnitude difference between the secondary and primary shows that the J-band "bump" is indeed a real feature and not an artifact caused by unresolved binarity.

Subject headings: binaries: general, close { stars: individual (2MASS J11061197+ 2754225, 2MASS J14044941 3159329) { stars: low-mass, brown dwarfs { techniques: high angular resolution, spectroscopy

1. INTRODUCTION

As brown dwarfs cool and pass through the L/T spectral class boundary, their spectral morphologies transition from red near-infrared (NIR) colors of the L dwarf class, caused by condensate dust in their photospheres, to blue NIR colors of the T dwarf class, where their photospheres are relatively clear of dust. This transition is rapid, as implied by the nearly effective temperature scale around 1400 K for NIR L7/T5 dwarfs (Golimowski et al. 2004; Kirkpatrick 2005, bottom panel of Fig. 7 in that paper). Within this transition, a remarkable brightening in J-band ($M_J - 1$) from spectral types T1–T5, known as the J-band "bump" (Dahn et al. 2002; Tinney et al. 2003; Viba et al. 2004), has been noted.

Two withstanding mechanisms to explain this brightening have been suggested: (1) the "patchy clouds" model { proposed by Burgasser et al. (2002) (see also Ackerman & Marley 2001), suggesting that the break-up of clouds in the atmosphere allows hot flux from inner layers to emerge (analogous to the 5 μm hot spots of Jupiter), and (2) the "sudden downpour" model { proposed by Knapp et al. (2004), suggesting that the dust clouds suddenly condense out due to an increase in sed-

imentation efficiency.

Recent studies of brown dwarf binaries have revealed that a fraction of the amplitude in this bump can be explained by systems appearing overluminous due to binarity (i.e., "crypto-binarity"; Burgasser et al. 2006b; Liu et al. 2006; Burrows et al. 2006); however, some part of this brightening is intrinsic to the atmospheres as they cool. This was revealed by HST/WFPC2 imaging of 2MASS J17281150+ 3948593AB (hereafter 2MASS 1728AB), the first 1.2 μm flux reversal binary, which has a T dwarf secondary brighter in z-band but fainter in i-band than the mid-to-late-type L dwarf primary (Gizis et al. 2003). No J-band resolved photometry for this system has been published. Two later discoveries of 1.2 μm flux reversal binaries { SDSS J102109.69 030420.1 (hereafter SDSS 1021; HST/NICMOS, Burgasser et al. 2006b) and SDSS J153417.05+ 161546.1 (hereafter SDSS 1534; Keck LGS AO/NIRC2, Liu et al. 2006) { provided additional information on the flux reversals. Both systems were found to have a secondary brighter than the primary in J-band (see Table 1).

L dwarf/T dwarf binaries such as those listed above provide crucial information on the L/T transition, as the components of these systems are likely coeval, with common ages and compositions. In an effort to identify additional systems, we have performed high angular resolution imaging of two T2.5 dwarfs { 2MASS J11061197+ 2754225 (hereafter 2MASS 1106) and 2MASS J14044941 3159329 (hereafter 2MASS 1404). These objects were identified in a NIR proper motion survey (Looper et al. 2007; Kirkpatrick et al., in prep) based on multi-epoch data from the Two Micron All Sky Survey (2MASS; Skrutskie et al. 2006). Both systems are in the field, unassociated with any higher mass stars within a radius of 10 arcminutes⁶. 2MASS 1404 was discovered to be a fourth resolved L/T transi-

¹ Some of the data presented herein were obtained at the W. M. Keck Observatory, which is operated as a scientific partnership among the California Institute of Technology, the University of California and the National Aeronautics and Space Administration. The Observatory was made possible by the generous financial support of the W. M. Keck Foundation. This paper includes data gathered with the 6.5-m Magellan Telescopes located at Las Campanas Observatory, Chile.

² Institute for Astronomy, University of Hawaii, 2680 Woodlawn Dr., Honolulu, HI 96822

³ Spitzer Science Center, M/S 220-6, California Institute of Technology, Pasadena, CA 91125

⁴ MIT Kavli Institute for Astrophysics & Space Research, 77 Massachusetts Ave, Building 37-664B, Cambridge, MA 02139

⁵ Infrared Processing and Analysis Center, M/S 100-22, California Institute of Technology, Pasadena, CA 91125

⁶ See <http://simbad.u-strasbg.fr/simbad/>.

tion system showing this 1.2 m flux reversal. These observations were made using the Keck II sodium laser guide star adaptive optics system. We describe these observations and optical spectroscopy of 2M ASS 1404 in x2, discuss the results of this imaging and implications for the J-band bump in x3, and give our conclusions in x4.

2. OBSERVATIONS

2.1. High Resolution Imaging: Keck II 10.0-m /NIRC2 LGS AO

We used the Keck II 10.0 m Telescope⁷ Sodium Laser Guide Star Adaptive Optics (LGS AO) system (Wizinowich et al. 2006; van Dam et al. 2006) on 2006 June 3 UT to observe 2M ASS 1106 and 2M ASS 1404. Observations were taken using the NIRC2 narrow camera and the Mauna Kea Observatories (MKO) filter set (Tokunaga et al. 2002): K_s -band (2.15 μ m) for 2M ASS 1106 and J (1.25 μ m), H (1.635 μ m), and K_s -bands for 2M ASS 1404. The field of view was $10''$ with a $0''.00994$ pixel scale. Nearby ($< 60''$) and bright ($R < 19$ mag) stars were selected from the USNO-B1.0 catalog (Monet et al. 2003) to provide for tip-tilt (TT) sensing. For 2M ASS 1106, the TT star (USNO-B1.0 1179-0233699) had a brightness of $R = 15.2$ mag and a separation of $52''$. For 2M ASS 1404, the TT star (USNO-B1.0 0580-0365843) had a brightness of $R = 16.3$ mag and a separation of $29''$. Conditions were clear and photometric with good seeing at the start of the night ($0''.7$ at K -band) with slight degradation afterwards.

For 2M ASS 1106, we dithered by a few arcseconds between positions to obtain a set of eight images with an integration time of 60 sec for each position, for a total on-source integration time of 480 sec. For 2M ASS 1404, we dithered by a few arcseconds between positions, for a total of six images for each of the three filters. Integration times per position were 90 sec, 60 sec, and 60 sec for a total integration time of 540 sec, 360 sec, and 360 sec in the J, H, and K_s filters, respectively. The full widths at half maximum (FWHM) in the K_s filter were $0''.068$ and $0''.065$ for 2M ASS 1106 and 2M ASS 1404, respectively.

We employed standard reduction techniques. Flats were created from dithered lights-on and lights-off images of the telescope dome interior. A super-sky frame was created from the median of the individual science frames and was subsequently subtracted from each frame. The background subtracted images were shifted so that the target landed on the same position and were then stacked to form the nal mosaic.

In the mosaic of 2M ASS 1106 (see Fig. 1), the target is not elongated and no other objects, companions or background sources, are seen. On the other hand, we have resolved 2M ASS 1404 into two components, shown in Fig. 2. Based on the large proper motion of this system ($\mu = 0''.35$ yr⁻¹) and the elapsed 5.3 yrs between the first 2M ASS observation of this field (2001 Feb 4 UT) and our observation with Keck II (2006 Jun 3 UT), we should be able to see both components separated in the 2M ASS image, which has a plate scale of $1''$, if they were not physically associated. Because we do not see an object on the 2001 2M ASS image that is positionally coincident with the double seen in our 2006 Keck

image, we conclude that this is a physical binary unresolved in 2M ASS images. Using the K_s -band nal mosaic, which has the smallest FWHM, we find a separation, θ , of $0''.1336 \pm 0''.0006$ and a position angle, ϕ , of 311.8 ± 0.7 .

We performed an image subtraction technique in all three bands to obtain nal flux ratios for the 2M ASS 1404AB system. To do this, we computed the centroid for the component to be subtracted and placed this component at the center of a 257×257 pixel subimage. This subimage was copied, rotated 180 degrees, and then subtracted from the original, non-rotated subimage. The quality of the subtraction was checked both visually and by examination of the radial profile of the unsubtracted component. In many cases, small offsets had to be applied by hand to obtain optimal subtraction. A aperture photometry was performed on the unsubtracted objects and used to obtain the flux ratio difference of the components.

Errors in the rotation-subtraction technique were estimated by creating fake binaries from (presumably) single objects observed with NIRC2 in LGS AO mode and having similar image qualities as 2M ASS 1404AB. The fake binaries were created at 25 different separations and position angles. The same rotation-subtraction technique was performed on these binaries as was done for 2M ASS 1404AB. The magnitude of each component was taken to be the average of the 25 separate measurements and the error was the standard deviation of the measurements.

The nal errors in the photometry for 2M ASS 1404AB are the square root of the sum of squares for the following eight terms: the errors in the single point-spread function (PSF) photometry (both A and B), the standard deviation of the binary PSF photometry (both A and B), the difference between the single and binary PSF photometry (both A and B), and the errors in 2M ASS 1404AB photometry (both A and B). The nal flux ratios for 2M ASS 1404AB are shown in Table 2.

2.2. Red Optical Spectroscopy: Magellan 6.5-m /LDSS3

Red optical spectroscopy ($6000\text{--}10500 \text{ \AA}$) of the 2M ASS 1404AB system was obtained on 2006 May 8 (UT) with LDSS-3 (upgraded from LDSS-2, Allington-Smith et al. 1994) on the 6.5-m Magellan Clay Telescope. Conditions were clear with good seeing ($0''.6$ at R -band). The VPH-red grism (660 lines/mm) and the OG590 longpass filter were used with a $0''.75$ (4 pixels) slit, resulting in $R = 1800$. The slit was rotated to the parallactic angle to minimize slit losses. Dispersion across the chip was 1.2 \AA/pixel . We obtained two exposures of 1500 sec each, for a total integration time of 50 minutes at an average airmass of 1.01. The flux standard star LTT 7987 (Hamuy et al. 1994) was observed the previous night (2006 May 7 UT) using an identical set-up. Calibration exposures were taken using the HeNeAr arc lamp and the at-field quartz lamp. The G2V star HD 127526 was observed immediately prior to 2M ASS 1404AB to use as a correction for telluric absorption.

LDSS-3 data were reduced in the IRAF⁸ environment. Raw science images were first trimmed, bias-subtracted

⁷ Located on the summit of Mauna Kea, Hawaii.

⁸ IRAF is distributed by the National Optical Astronomy Observatories, which are operated by the Association of Universities

and then divided by the normalized, median-combined and bias-subtracted set of standard frames. Spectra were optimally extracted using the APALL task, with the extraction of HD 127526 used as a dispersion template for 2M ASS 1404AB. Wavelength solutions were determined from the arc lamp spectra; solutions were accurate to

0.1 pixels, or 0.12 Å. Flux calibration was determined using the tasks STANDARD and SENSFUNC with observations of LTT 7987, adequate over the spectral range 6000{10000 Å. Corrections to telluric O₂ (6860{6960 Å B-band, 7580{7700 Å A-band) and H₂O (7150{7300 and 9270{9675 Å) absorption bands were computed using the G dwarf spectrum.

The optical spectrum is shown in Fig. 3, along with the L8 optical standard 2M ASS J1632291+190441 (hereafter 2M ASS 1632, Kirkpatrick et al. 1999) and the T2 optical standard SDSS J125453.90-012247.4 (hereafter SDSS 1254, Burgasser et al. 2003b) for comparison. The spectra are shown on a log flux scale and have been smoothed to R = 1000 to match the resolution of 2M ASS 1632 observed with Keck/LRIS. Overall, the continuum of 2M ASS 1404AB is intermediate between the L8 and T2 standards, consistent with an optical spectral type of T0. The inset box in this same figure shows the Cs I lines and FeH/CRH bands between 8400 and 9100 Å. The spectra shown in this inset have been divided through by a 4th-order polynomial fit to the continuum in order to highlight the strength of these features. The Cs I lines are of comparable strength in 2M ASS 1404AB as in SDSS 1254, while the FeH/CRH band in 2M ASS 1404AB is intermediate between the L8 and T2 standards. We therefore adopt an optical spectral type of T0 ± 1 for the 2M ASS 1404AB system.

3. ANALYSIS

3.1. New M_{JHK_s}-Spectral Type Relations Based on 2M ASS Photometry

We have derived JHK_s absolute magnitude versus spectral type relations using optically classified late-type M and L dwarfs and NIR classified T dwarfs with parallax measurements of signal-to-noise ratio (S/N) > 5 and not known to be binary (collected from: Perryman et al. 1997; Dahn et al. 2002; Tinney et al. 2003; Vrba et al. 2004). The coefficients of the sixth-degree polynomial fits to this unweighted data are given in Table 3 and shown graphically in Fig. 4. We have used optical spectral classification for the L dwarfs because no formal L dwarf NIR spectral classification scheme has been constructed⁹. These relations use the new NIR spectral classification scheme for T dwarfs Burgasser et al. (2006a), superseding previous M_{JHK} versus spectral type (SpT) relations on the old NIR T dwarf scheme (Geballe et al. 2002; Burgasser et al. 2002).

3.2. Component Spectral Types of 2M ASS 1404AB

Since the relative J- and H-band photometry is on the MKO photometric system and the relative K-band photometry is on the 2M ASS photometric system, we

for Research in Astronomy, Inc., under cooperative agreement with the National Science Foundation.

⁹ Geballe et al. (2002) have identified classification indices based on NIR molecular absorption bands.

need to convert the K-band photometry onto the same MKO system. To do this, we examined a set of 25 L6.0{T2.0 dwarfs, described below, and computed the (2M ASS MKO) K-band color term as 0.01 ± 0.04 averaged over these spectral classes. We show the breakdown of this color term per spectral class in Table 4. Since this color term difference is near zero, we assume the two are equivalent and proceed to determining the component MKO photometry, using the following steps:

1. Convert J_{AB} (2M ASS) to J_{AB} (MKO) using the (MKO 2M ASS) color term computed from the spectrum of 2M ASS 1404AB (Looper et al. 2007). J_{AB} (MKO 2M ASS) = 0.17; J_{AB} (MKO) = 15.41 ± 0.07.
2. Decompose the system: J_A = J_{AB} + 2.5 log(1 + 10^{0.4(J_B - J_A)}); $\frac{J_A}{J_B} = \frac{J_{AB}}{J_B} + \frac{2}{(10^{0.4(J_B - J_A)} - 1)^2}$, where J = J_A - J_B. J_A (MKO) = 16.46 ± 0.12.
3. Similarly, J_B = J_{AB} + 2.5 log(1 + 10^{0.4(J_A - J_B)}); $\frac{J_B}{J_A} = \frac{J_{AB}}{J_A} + \frac{2}{(10^{0.4(J_A - J_B)} - 1)^2}$, where J = J_A - J_B. J_B (MKO) = 15.93 ± 0.09.

In the same manner, this procedure was carried out to determine the MKO H-band and K-band component photometry (see Table 5).

To estimate NIR spectral types for the AB components, we compared the integrated light spectrum to a suite of synthetic IRTF/SpEx spectra constructed in the same manner as Burgasser et al. (2008). The constituents for these synthetic spectra are the 25 L6-T2 dwarfs, used for the primaries, and the 38 T3-T8 dwarfs, used for the secondaries, as listed in Burgasser et al. (2008)¹⁰, which is drawn from Burgasser et al. (2004, 2006a,c); Burgasser (2007); Chiu et al. (2006); Cruz et al. (2004); Liebert & Burgasser (2007); Looper et al. (2007); Reid et al. (2006); Siegler et al. (2007). In cases where more than one spectrum for an object was available, we used the highest SNR spectrum available. All combinations of primary and secondary were scaled together using the M_J magnitude from the M_J-SpT relation derived above in §3.1. This resulted in 1000 synthetic spectra. To estimate the goodness of fit between the data (2M ASS 1404AB) and each model, we first interpolated the flux of the models onto the wavelength scale of the data and normalized each to their peak flux over the 1.2{1.3 μm window. We then calculated the χ² values¹¹ between the data and each model over the wavelength ranges 0.95{1.35 μm, 1.45{1.8 μm, and 2.0{2.35 μm to avoid low S/N regions of the spectra. In addition, we calculated χ² for a range of multiplicative scale factors

¹⁰ Also, see <http://web.mit.edu/ajp/www/browndwarfs/spexprism/html/binaries> for a list of these 63 spectra, where we have eliminated 2M ASS J21513839-4853542 (T4) and 2M ASS J05103520-4208140 (T5) from the list of T3-T8 dwarfs used due to the poor signal-to-noise ratio (SNR) of their spectra.

¹¹ Defined as $\chi^2 = \sum \left(\frac{f(1404AB) - f(M)}{\sigma(M)} \right)^2$, where f(1404AB) is the data for 2M ASS 1404AB, f(M) is the synthetic model spectrum, and σ(M) are the errors in the data for 2M ASS 1404AB. The summation is performed over the wavelengths 0.95{1.35, 1.45{1.8, and 2.0{2.35 μm.

(0.5 to 1.5) of the data, in steps of 0.01, to eliminate the normalization bias, selecting the normalization that yielded χ^2_{\min} .

From the 1000 model spectra, we selected the 15 spectra with the smallest χ^2 values for visual inspection. The model spectrum created from SDSS J205235.31 160929.8 (T1, hereafter SDSS 2052; Chiu et al. 2006) for the primary and from 2MASS J23312378 4718274 (T5, hereafter 2MASS 2331; Burgasser et al. 2004) for the secondary with the same normalization provided the best fit and yielded 2MASS

$J = 0.18$ mag. We also examined model combinations constructed from two earlier type (L9 and T0) and two later type (T1.5 and T2) primaries with a T5 used as the secondary. In addition, we examined model combinations constructed from a T1 as the primary and two earlier type (T4 and T4.5) and two later type (T5.5 and T6) secondaries. Since any spectra with identical spectral types were available, we used those with model spectra that minimized χ^2 . All fits are shown in Fig. 5. The best fit is clearly the T1/T5 model, which shows an excellent match to the data of 2MASS 1404AB over all wavelengths. Deviating the spectral type of either the primary or secondary by a subtype or more while holding the other fixed, results in a degraded goodness of fit to the data. We therefore estimate a final NIR spectral type of the primary as T1 and of the secondary as T5.

Using the MKO component photometry of 2MASS 1404AB and component spectral type estimates of T1 and T5, we compute the 2MASS component photometry (see Table 5) using the appropriate transformations from Stephens & Leggett (2004). These relations are dependent on spectral type with errors that add negligibly to the component photometric errors. We can compare the relative 2MASS J-band photometry obtained from imaging, $J = 0.45 \pm 0.15$, to that obtained from our synthetic spectral modeling, $J = 0.18$, using a T1 primary and a T5 secondary. The relative 2MASS J-band photometry obtained from our synthetic spectral modeling is 1.8 sigma from our relative 2MASS J-band photometry obtained from imaging. It confirms that the secondary is indeed brighter than the primary in J-band.

As a check on our spectral type estimates, we compute 2MASS NIR colors of each component and compare these to the 2MASS NIR colors of published L and T dwarfs¹² in Fig. 6. In this color-color diagram, component A is seen coincident with a cluster of L7 T1 dwarfs. Component B is associated with a cluster of T4 T6 dwarfs. This color comparison yields an average spectral type estimate of L9 for component A and T5 for component B.

In Fig. 7, we plot SDSS 2052 and 2MASS 2331 scaled with the relative photometry of the A and B components of 2MASS 1404AB, with the 2MASS and MKO filter transmission profiles overlaid. The 2MASS J-band filter profile extends to slightly shorter wavelengths, covering more of the CH₄ absorption band at 1.15 μ m, than does the MKO J-band profile. This explains the reduced relative 2MASS J-band photometry of the two components compared to the relative MKO J-band photometry, since the secondary (T5) has larger CH₄ absorption than does

the primary (T1). The flux peaks, however, are more illuminating than the broadband photometry. The peak at 1.25 μ m of the scaled T5 is 70% brighter than that of the scaled T1, and the 1.05 μ m peak (outside the J-band filter profile) is 40% brighter. This redistribution of flux into the 1.05 and 1.25 μ m peaks is remarkably similar to that seen for SDSS 1021AB and SDSS 1534AB. SDSS 1021B is 30% and 25% brighter at the 1.25 and 1.05 μ m bands than SDSS 1021A, respectively. Likewise, SDSS 1534B is 30% and 20% brighter at the 1.25 and 1.05 μ m bands than SDSS 1534A. While no atmospheric models can accurately reproduce this flux redistribution, we refer the reader to Burgasser et al. (2006b) for a qualitative description of how this brightening may arise.

3.3. Construction of Color-Magnitude Diagrams

Using the new M_{JHK_s} -SpT relations derived in x3.1, we estimate distances for component A, assuming a T1 spectral type, of 25.8, 22.6, and 20.2 pc, respectively, yielding a mean distance of 23 pc. We can now place 2MASS 1404AB and its components on a color-magnitude diagram (see Fig. 4). Likewise, SDSS 1021AB and SDSS 1534AB are also shown, and these have been converted onto the 2MASS photometric system using the spectral type estimates of their components, their component MKO photometry, and the appropriate transformations from Stephens & Leggett (2004). The parallax measurement for SDSS 1021AB (Tinney et al. 2003) is used to place it on the diagram. Since SDSS 1534AB lacks a parallax measurement, we use the M_{JHK_s} -SpT relations for component SDSS 1534A ($d_{\text{est}} = 41$ pc) to place SDSS 1534AB on the diagram.

Of note, only two other T dwarfs in the J-band bump, SDSS J175032.96+175903.9 (T3.5; hereafter SDSS 1750) and 2MASS J05591914 1404488 (T4.5; hereafter 2MASS 0559), lie above the J-band bump, by 0.3 and 0.9 mag, respectively. Neither object has been resolved in high-angular resolution studies (Burgasser et al. 2006b, 2003a), nor show any signs of unusual metallicity or gravity effects in their spectra. These objects could still be binaries with very small separations and/or imaged at an unpropitious place in their orbits, as was originally the case with Kelu-1 (Liu & Leggett 2005; Gelino et al. 2006). However, Zapatero Osorio et al. (2007) have monitored 2MASS 0559 over a period of 4.37 years with radial velocity measurements and have ruled out companions more massive than 10 M_{Jup} in orbits of 1 yr and companions more massive than 2 M_{Jup} in orbits of less than a few days.

In order to eliminate the J-band bump, SDSS 1750 would have to be an unresolved binary, 2MASS 0559 would have to be an unresolved triple (since $J > 0.75$ mags) with the above restrictions on the orbital periods of its components, and 2MASS 1404AB would also have to be a triple system instead of a binary. The small observed frequency of brown dwarf triple systems ($3^{+4}_{-1}\%$ {not considering selection effects; Burgasser et al. 2007) suggests this is highly unlikely. Hence, the amplitude of the J-band bump is probably at least 0.5 mag as illustrated by the components of 2MASS 1404AB and likely as high as 1 mag in light of the recent null result of radial velocity companions to 2MASS 0559 by Zapatero Osorio et al. (2007). A parallax measurement

¹² See <http://dwarfarchives.org>.

and resolved spectroscopy of this system are needed to accurately place the components on a color magnitude diagram. Radial velocity monitoring of the 2M ASS 1404AB system can resolve if this brightening is intrinsic to the atmospheres as they cool or if higher-order multiplicity is responsible for this peculiar flux reversal at $1.12 \mu\text{m}$.

3.4. Physical Parameters of 2M ASS 1404AB

To estimate the physical parameters of 2M ASS 1404AB (see Table 2), we first derived MKO K-band bolometric corrections (BC_K) versus spectral type and T_{eff} versus spectral type relations, using M 9{T8 data from Golimowski et al. (2004) and references therein, excluding known binaries. In both relations, we classify L dwarfs on the Kirkpatrick et al. (1999) optical classification scheme, and T dwarfs on the Burgasser et al. (2006a) NIR classification scheme. Our choice of optical L dwarf spectral classification for these stars is further strengthened because the far-optical spectrum of mid-to late-type L dwarfs is less influenced by cloud opacities than the Geballe et al. (2002) $1.5 \mu\text{m}$ H_2O index (Knap et al. 2004). The coefficients to the fourth-degree weighted BC_K polynomial fit and to the sixth-degree unweighted T_{eff} polynomial fit are given in Table 3 and shown graphically in Fig. 8. The stars in this fit (87 K) compared to that of Golimowski et al. (2004) (124 K) is less because of the elimination of objects found to be binary between the time of that publication and this paper. Using the T_{eff} -SpT relation, we estimate effective temperatures of 1390 ± 90 K and 1180 ± 90 K for the primary and secondary, respectively, assuming an age of 3 Gyr. We also find BC_K values of 2.91 ± 0.16 and 2.34 ± 0.16 for the primary and secondary, respectively. In both cases, the error is the RMS in the fit and does not include the error in spectral typing.

To determine M_{bol} for each component, we used the BC_K corrections, a distance estimate of $d = 23$ pc, and the MKO component photometry (see Table 5). This yielded $M_{\text{bol}} = 15.96 \pm 0.19$ mag and 16.59 ± 0.25 mag for the primary and secondary, respectively. The ratio of bolometric luminosities, $L_{\text{bol},A}/L_{\text{bol},B}$, is 1.79 ± 0.52 , with the primary having the higher luminosity. We use their mass-luminosity relation $L_{\text{bol}}/M^{2.64}$ (Burrows et al. 2001), which assumes solar metallicities, and the ratio of bolometric luminosities to find the mass ratio: $q = M_B/M_A = 0.80 \pm 0.09$. This mass ratio is typical for known brown dwarf binaries, which tend to peak at $q \approx 1$ (73% of observed binaries have $q < 0.8$, although, observational bias would favor high- q ratios; Burgasser et al. 2006b). Using the age-luminosity relation from Burrows et al. (2001), we find a total mass for the system of 50, 70, and $80 M_{\text{Jup}}$, corresponding to ages of 0.5, 1.0, and 5.0 Gyr, typical for local disk dwarfs (Reid & Hawley 2000). This corresponds to individual masses of 28 and $22 M_{\text{Jup}}$, 39 and $31 M_{\text{Jup}}$, and 44 and $36 M_{\text{Jup}}$ for these respective ages.

Finally, this allows determination of the orbital parameters of this system. At an estimated distance of 23 pc and with an apparent separation of $0''.134$, the projected physical separation is 3.1 AU . Statistically, the true semimajor axis can then be estimated as

$a = 1.26 \pm 3.9 \text{ AU}$ (Fischer & Marcy 1992). This implies an orbital period of roughly 28–35 yr, assuming a total system mass of $50–80 M_{\text{Jup}}$.

4. CONCLUSIONS

We have presented high resolution imaging of two T2.5 dwarfs { 2M ASS 1106 and 2M ASS 1404 } and resolved the latter into a $0''.13$ binary. 2M ASS 1404AB is an intriguing binary as its presumably cooler secondary is brighter in J-band than the primary by 2M ASS J = 0.45 mags but fainter in both 2M ASS H- (by 0.49 mags) and 2M ASS K_s-bands (by 1.13 mags). This secondary brightening in J-band is much more pronounced than that seen in the other two known flux reversal binaries with resolved J-band photometry { SDSS 1021 (2M ASS J = 0.05, MKO J = 0.04) and SDSS 1534 (2M ASS J = 0.03, MKO J = 0.17). Zapatero Osorio et al. (2007) have found no companions in their radial velocity monitoring of the T4.5 dwarf 2M ASS 0559, which lies 0.9 mag above the 2M ASS M_J versus spectral type relation we derive. This result in conjunction with ours suggest that a brightening of at least 0.5 mag and likely as high as 1 mag in the J-band bump is real and intrinsic to the atmospheres of these objects as they cool across early-to mid-type T classes.

5. ACKNOWLEDGMENTS

We thank our anonymous referee for comments which improved this manuscript. We would like to thank our telescope operators on Keck: Jim Lyke, Cynthia Wilbum, Chuck Sorenson, and the rest of the Keck LGS AO team and our telescope operator on Magellan: Mauricio Martinez. We thank Michael Liu for the LGS AO data on these two sources, and Michael Cushing and Mark Pitts for helpful discussions. D.L.L. thanks Michael Liu and John Rayner for advising her for this project, and David Sanders for financial support. This research has made use of the SIMBAD database, operated at CDS, Strasbourg, France. This research has benefited from the M, L, and T dwarf compendium housed at DwarfArchives.org and has used data products from the SpeX Prism Spectral Libraries (<http://www.browndwarfs.org/speXprism>). This publication also makes use of data products from the Two Micron All Sky Survey (2MASS), which is a joint project of the University of Massachusetts and the Infrared Processing and Analysis Center/California Institute of Technology, funded by the National Aeronautics and Space Administration and the National Science Foundation. This research has also made use of the NASA/IPAC Infrared Science Archive (IRSA), which is operated by the Jet Propulsion Laboratory, California Institute of Technology, under contract with the National Aeronautics and Space Administration. As all data were obtained from the summit of Mauna Kea, the authors wish to recognize and acknowledge the very significant cultural role and reverence that this mountaintop has always had within the indigenous Hawaiian community. We are most fortunate to have the opportunity to conduct observations on the summit.

Facilities Used: Keck-II, Magellan-Clay.

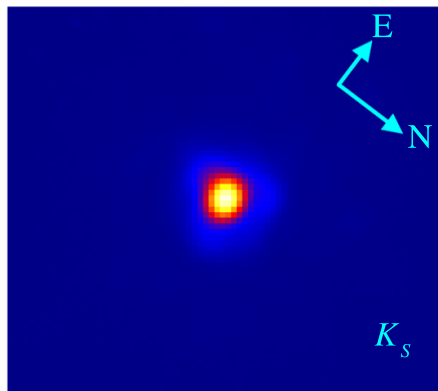


Fig. 1. | Keck LGS AO image of 2MASS 1106 in K_s band. North and East are indicated by an arrow. The image is $0''.8$ on a side, with no other sources besides the target detected in the full-sized ($13''.5$) field-of-view. The FWHM is $0''.068$.

REFERENCES

- Ackerman, A. S., & Marley, M. S. 2001, *ApJ*, 556, 872
- Allington-Smith, J., et al. 1994, *PASP*, 106, 983
- Burgasser, A. J., Liu, M. C., Ireland, M. J., Cruz, K. L., & Dupuy, T. J. 2008, *ArXiv e-prints*, 803, arXiv:0803.0295
- Burgasser, A. J. 2007, *ApJ*, 659, 655
- Burgasser, A. J., Reid, I. N., Siegler, N., Close, L., Allen, P., Lowrance, P., & Gizis, J. 2007, *Protostars and Planets V*, 427
- Burgasser, A. J., Burrows, A., & Kirkpatrick, J. D. 2006c, *ApJ*, 639, 1095
- Burgasser, A. J., Kirkpatrick, J. D., Cruz, K. L., Reid, I. N., Leggett, S. K., Liebert, J., Burrows, A., & Brown, M. E. 2006b, *ApJS*, 166, 585
- Burgasser, A. J., Geballe, T. R., Leggett, S. K., Kirkpatrick, J. D., & Golimowski, D. A. 2006a, *ApJ*, 637, 1067
- Burgasser, A. J., McElwain, M. W., Kirkpatrick, J. D., Cruz, K. L., Tinney, C. G., & Reid, I. N. 2004, *AJ*, 127, 2856
- Burgasser, A. J., Kirkpatrick, J. D., Liebert, J., & Burrows, A. 2003b, *ApJ*, 594, 510
- Burgasser, A. J., Kirkpatrick, J. D., Reid, I. N., Brown, M. E., Miskey, C. L., & Gizis, J. E. 2003a, *ApJ*, 586, 512
- Burgasser, A. J., Marley, M. S., Ackerman, A. S., Saumon, D., Lodders, K., Dahn, C. C., Harris, H. C., & Kirkpatrick, J. D. 2002, *ApJ*, 571, L151
- Burrows, A., Sudarsky, D., & Hubeny, I. 2006, *ApJ*, 640, 1063
- Burrows, A., Hubbard, W. B., Lunine, J. I., & Liebert, J. 2001, *Reviews of Modern Physics*, 73, 719
- Chiu, K., Fan, X., Leggett, S. K., Golimowski, D. A., Zheng, W., Geballe, T. R., Schneider, D. P., & Brinkmann, J. 2006, *AJ*, 131, 2722
- Cruz, K. L., Burgasser, A. J., Reid, I. N., & Liebert, J. 2004, *ApJ*, 604, L61
- Dahn, C. C., et al. 2002, *AJ*, 124, 1170
- Fischer, D. A., & Marcy, G. W. 1992, *ApJ*, 396, 178
- Geballe, T. R., et al. 2002, *ApJ*, 564, 466
- Gelino, C. R., Kulkarni, S. R., & Stephens, D. C. 2006, *PASP*, 118, 611
- Gizis, J. E., Reid, I. N., Knapp, G. R., Liebert, J., Kirkpatrick, J. D., Koerner, D. W., & Burgasser, A. J. 2003, *AJ*, 125, 3302
- Golimowski, D. A., et al. 2004, *AJ*, 128, 1733
- Hamuy, M., Suntze, N. B., Heathcote, S. R., Walker, A. R., Gignoux, P., & Phillips, M. M. 1994, *PASP*, 106, 566
- Kirkpatrick, J. D. 2005, *ARA&A*, 43, 195
- Kirkpatrick, J. D., et al. 1999, *ApJ*, 519, 802
- Knapp, G. R., et al. 2004, *AJ*, 127, 3553
- Liebert, J., & Burgasser, A. J. 2007, *ApJ*, 655, 522
- Liu, M. L., Leggett, S. K., Golimowski, D. A., Chiu, K., Fan, X., Gellae, T. R., Schneider, D. P., & Brinkmann, J. 2006, *ApJ*, 647, 1393
- Liu, M. C., & Leggett, S. K. 2005, *ApJ*, 634, 616
- Looper, D. L., Kirkpatrick, J. D., & Burgasser, A. J. 2007, *AJ*, 134, 1162
- Monet, D. G., et al. 2003, *AJ*, 125, 984
- Osorio, M. R. Z., Marten, E. L., Bejar, V. J. S., Bouy, H., Deshpande, R., & Wainscoat, R. J. 2007, *ApJ*, 666, 1205
- Perryman, M. A. C., et al. 1997, *A&A*, 323, L49
- Reid, I. N., Lewin, E., Burgasser, A. J., & Cruz, K. L. 2006, *ApJ*, 639, 1114
- Reid, I. N., & Hawley, S. L. 2000, *New light on dark stars: red dwarfs, low mass stars, brown dwarfs* / Neill Reid and Suzanne L. Hawley. New York : Springer, 2000. (Springer-Praxis series in astronomy and astrophysics)
- Siegler, N., Close, L. M., Burgasser, A. J., Cruz, K. L., Marois, C., McIntosh, B., & Barman, T. 2007, *AJ*, 133, 2320
- Skrutskie, M. F., et al. 2006, *AJ*, 131, 1163
- Stephens, D. C., & Leggett, S. K. 2004, *PASP*, 116, 9
- Tinney, C. G., Burgasser, A. J., & Kirkpatrick, J. D. 2003, *AJ*, 126, 975
- Tokunaga, A. T., Simons, D. A., & Vacca, W. D. 2002, *PASP*, 114, 180
- van Altena, W. F., Lee, J. T., & Hoffeit, D. 1995, *VizieR Online Data Catalog*, 1174, 0
- van Dam, M. A., et al. 2006, *PASP*, 118, 310
- Vrba, F. J., et al. 2004, *AJ*, 127, 2948
- Wizinowich, P. L., et al. 2006, *Proc. SPIE*, 6272, 7

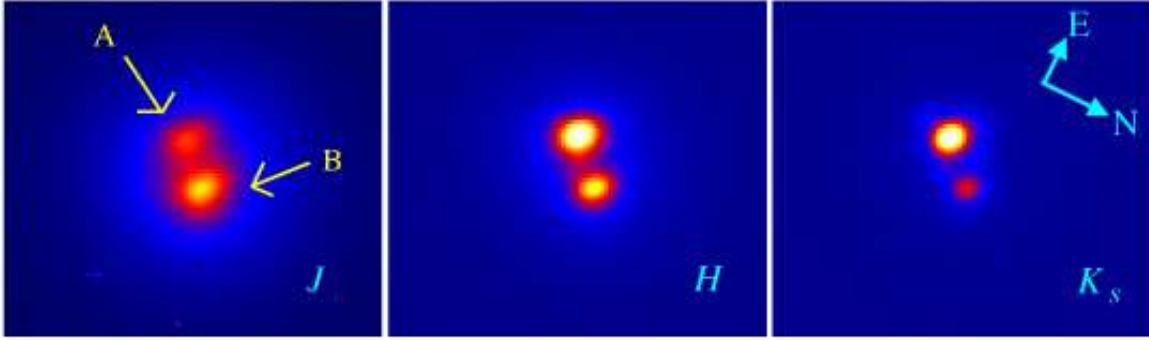


Fig. 2. | Keck LGS AO images of 2MASS 1404AB in J, H, and K_s bands. North and East are indicated by an arrow and is the same for all images. Note that the B component is brighter in J-band than the A component but is fainter in both H- and K_s -bands. Each subimage is $0''.8$ on a side, and the separation of the binary is $0''.1336 \pm 0''.0006$ with a position angle of $311.8 \pm 0.7^\circ$. No other sources besides components A and B were detected in the full-sized ($14''$) field-of-view. The FWHM is $0''.065$ in K_s -band.

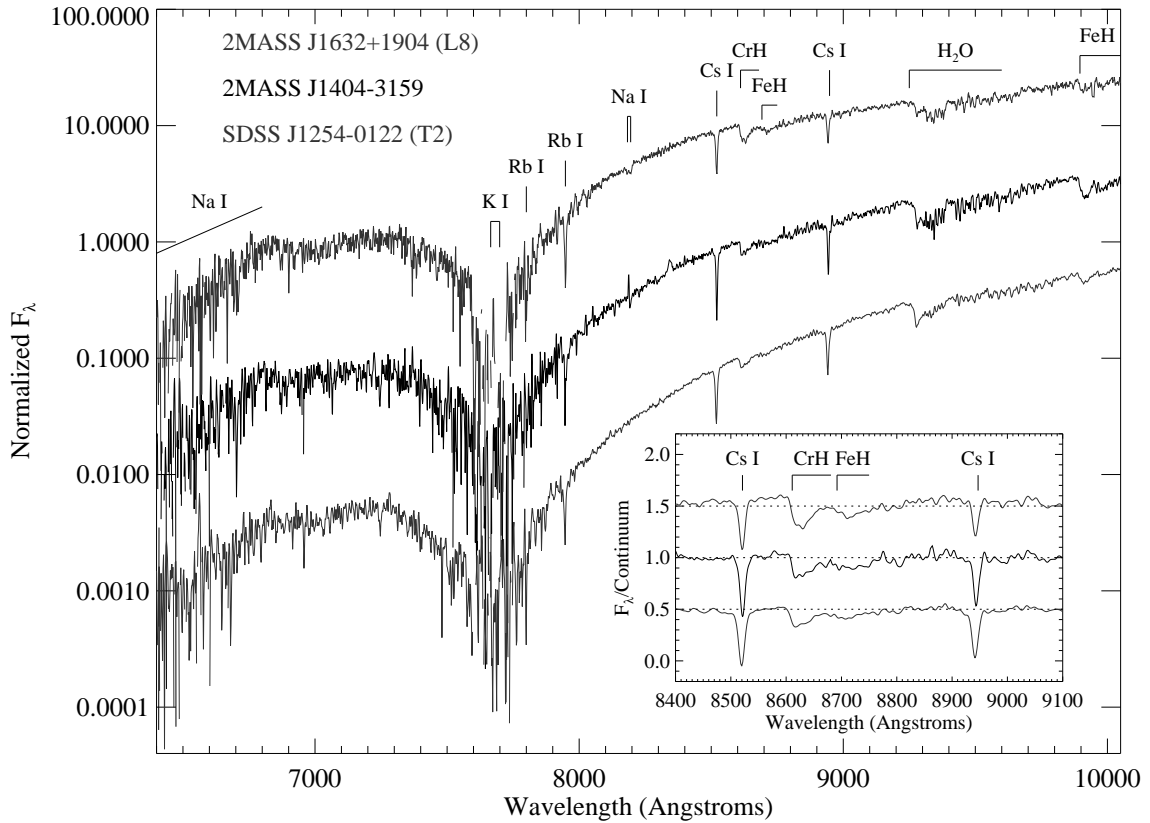


Fig. 3. | Red optical spectrum of 2MASS 1404AB (obtained with LDSS-3/Magellan; optical T0 = 1) in comparison to 2MASS 1632 (L8 optical standard; Kirkpatrick et al. 1999) and SDSS 1254 (T2 optical standard; Burgasser et al. 2003b) normalized and shown on a logarithmic scale. The insert shows the region between 8400–9100 Å, where the spectra have been divided by a 4th-order polynomial fit to the continua. 2MASS 1404AB and SDSS 1254 have been smoothed down to approximately the same resolution as 2MASS 1632 ($R \approx 1000$). Major atomic and molecular features are labeled, and the spectra are separated along the vertical axis for clarity. 2MASS 1404AB appears to be intermediate in type between the L8 and T2 optical standards.

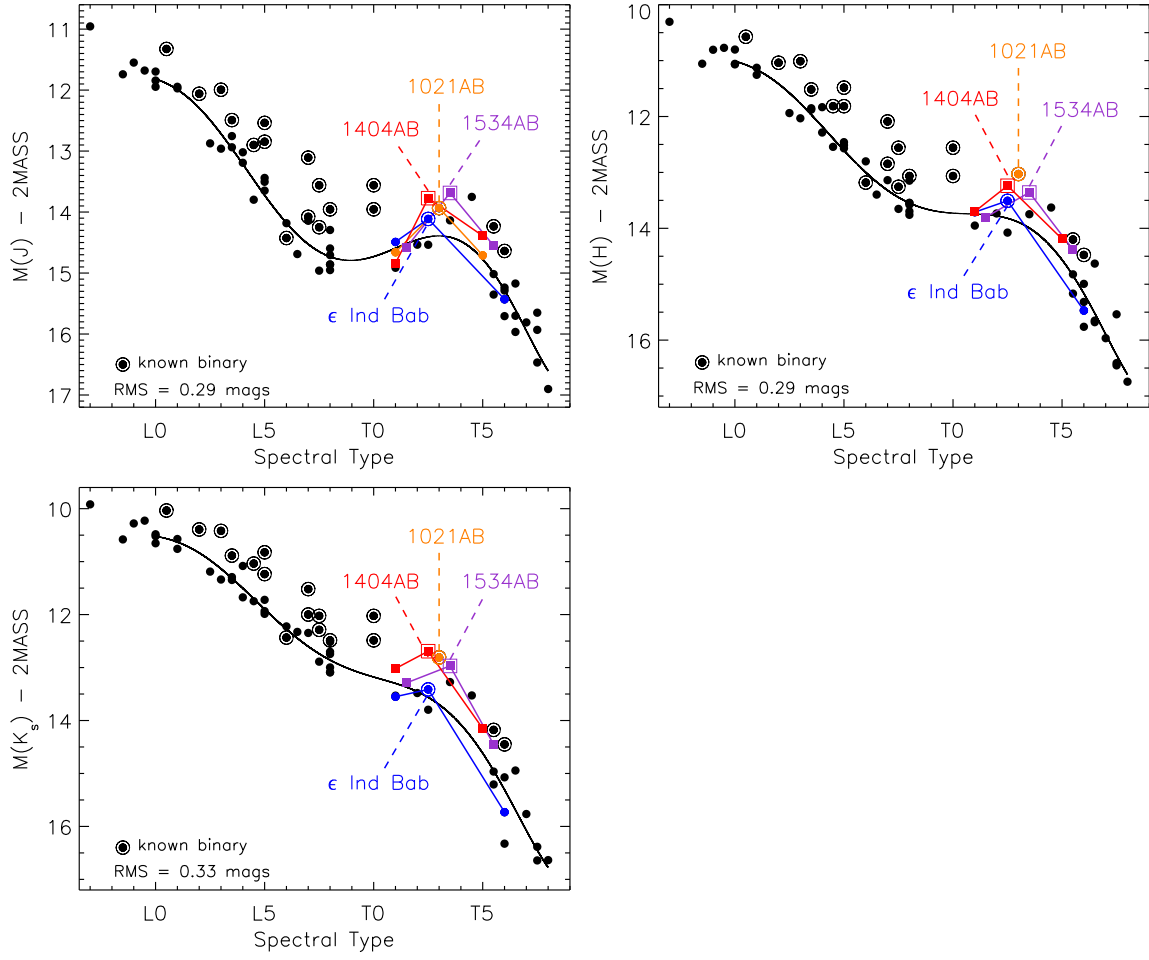


Fig. 4. | M_{JHK_s} -vs-SpT of optical L dwarfs (on Kirkpatrick et al. 1999 scheme) and NIR T dwarfs (on Burgasser et al. 2006a scheme) with parallax measurements of $\text{SNR} > 5$ (solid points). The (unweighted) sixth-degree polynomial fits defined in x3.1 are shown as solid lines. Late type M dwarfs were also included in these fits to prevent an artificial downturn at L0. Known binaries are encircled and were not included in the fit, with the exception of ϵ Ind Bab (blue), where the spectroscopically classified components have been used. Top: A clear brightening in M_J is seen from T1(T5, known as the J-band bump). The three known J-band flux reversal binaries (SD SS 1021AB, SD SS 1534AB, and 2MASS 1404AB) and their A+B components are shown as orange, purple, and red, respectively. 2MASS 1404AB and SD SS 1534AB are indicated by squares, not circles, since no parallax measurement has been made for either of these sources. No H- and K_s -band resolved photometry is available for SD SS 1021AB.

TABLE 1
J-Band Flux Reversal Binaries^a

Designation	J^{2MASS}		J_{AB}^{2MASSb}	J_{AB}^{MKOc}	SpT AB ^d	SpT A ^d	SpT B ^d	Ref ^e
SD SS 1021AB	16.25	0.09	0.05	0.04	T 3	T 1	T 5	1
SD SS 1534AB	16.75	0.13	0.03	0.17	T 3.5	T 1.5	T 5.5	2
2MASS 1404AB	15.56	0.09	0.45	0.53	T 2.5	T 1	T 5	3

^a There is one other (possible) J-band flux reversal binary not tabulated here: 2MASS 1728AB because it has been observed at z-band not at J-band (see x1).

^b Relative 2MASS photometry calculated in this paper.

^c Relative MKO photometry from references.

^d NIR spectral types on Burgasser et al. (2006a) scheme.

^e References { (1) Burgasser et al. (2006b), (2) Liu et al. (2006), (3) this paper.

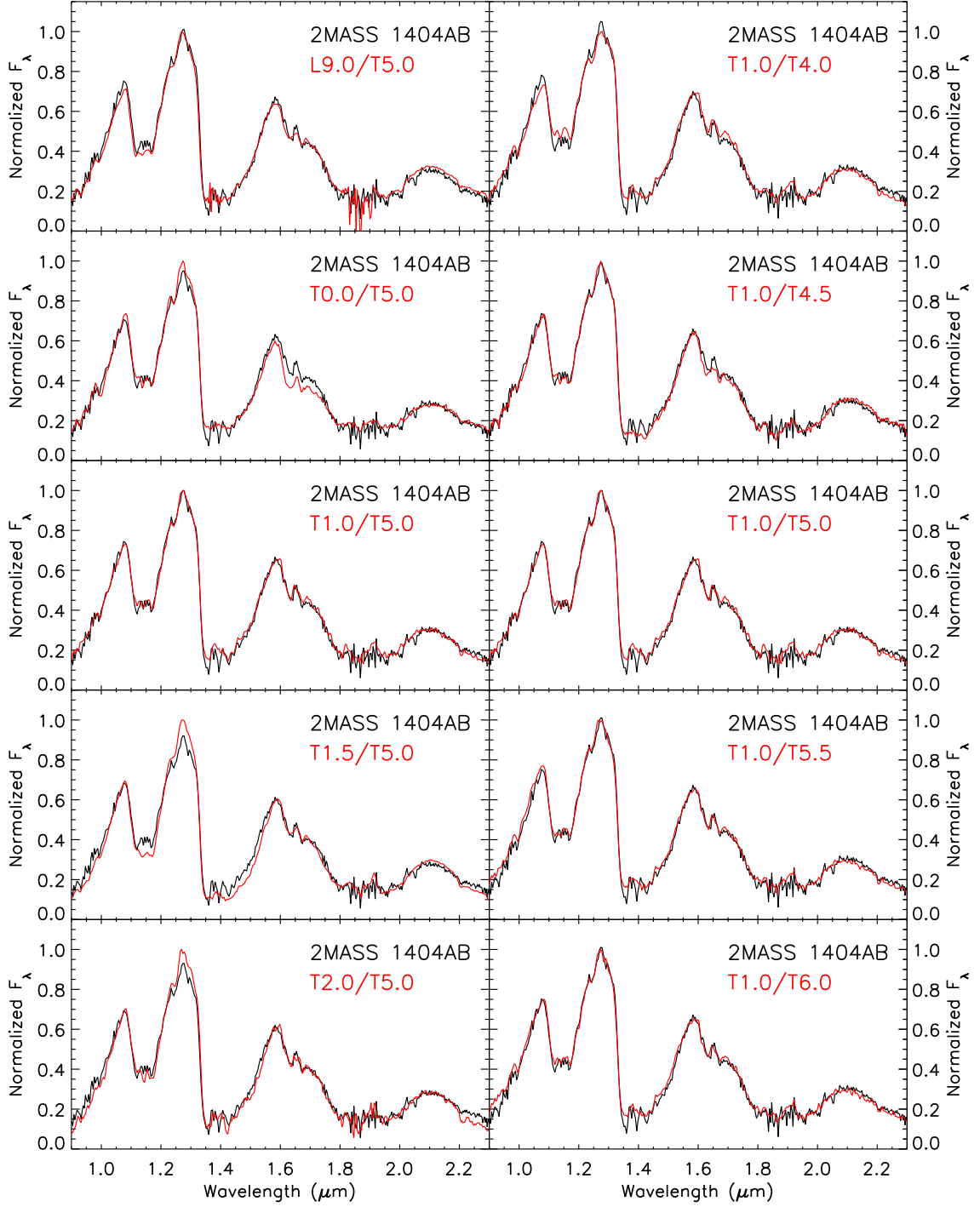


Fig. 5. Comparison of the T2.5 integrated light spectrum of 2MASS 1404AB (black;Looper et al.2007) with the best synthetic spectral types (red; see x3.2). The T1 and T5 combination provides the best fit across all wavelengths to the spectrum of 2MASS 1404AB.

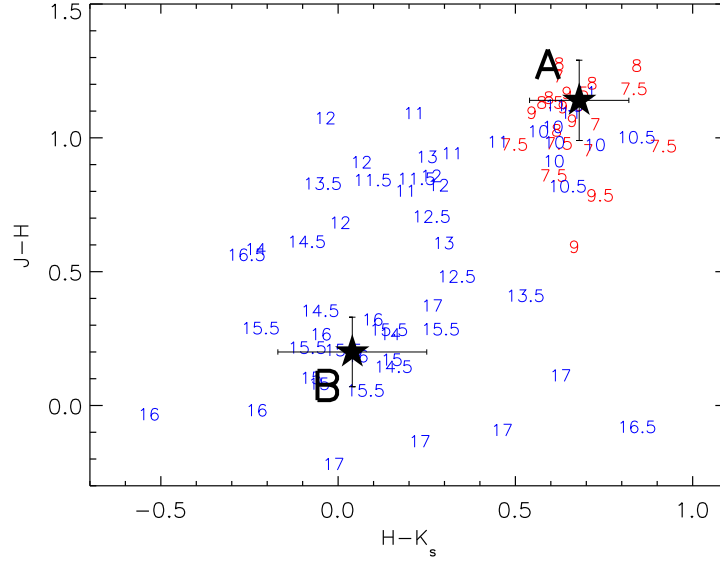


Fig. 6. NIR color-color plot of 74 known NIR L7-T7 dwarfs with $J-H$ and $H-K_s < 0.3$ mag and spectral types with uncertainties ± 1 subtype. L dwarfs are shown in red with spectral types represented by numbers 7 = L7, 8 = L8, etc. T dwarfs are shown in blue with spectral types represented by numbers 10 = T0, 15 = T5, etc. The resolved colors of 2M ASS 1404AB are shown as stars with associated error bars.

TABLE 2
Properties of the 2M ASS 1404AB System

Property	Value	
M KO J (mag)	15.41	0.07
M KO H (mag)	15.02	0.08
M KO K (mag)	14.55	0.10
M KO J (mag)	0.53	0.16
M KO H (mag)	0.48	0.11
M KO K (mag)	1.20	0.21
2M ASS J (mag)	15.58	0.07
2M ASS H (mag)	14.96	0.08
2M ASS K _s (mag)	14.54	0.10
2M ASS J (mag)	0.45	0.15
2M ASS H (mag)	0.49	0.13
2M ASS K _s (mag)	1.13	0.22
Composite Optical SpT	T0	
Composite NIR SpT	T2.5 ^a	
($^{\circ}$ yr ⁻¹)	0.35	0.03 ^a
(deg)	275.3	0.2 ^a
(mas)	133.6	0.6
(deg)	311.8	0.7
$\log(L_A/L_B)^b$	0.25	0.13
$q = M_B/M_A$	0.80	0.09
$M_{\text{tot}} (M_{\text{Jup}})$ for 0.5, 1.0 & 5.0 Gyr	50, 70 & 80	
Est: distance (pc)	23	
Est: projected separation (AU)	3.1	
Est: actual separation (AU)	3.9	
Orbital Period (yr)	28 ± 35	

^a Measurements are from Looper et al. (2007).

^b $\frac{L_{\text{bol}}}{L_{\text{bol}}} = 100^{(M_{\text{bol}} - M_{\text{bol}}^{\text{ref}})}$, where $M_{\text{bol}}^{\text{ref}} = +4.76$.

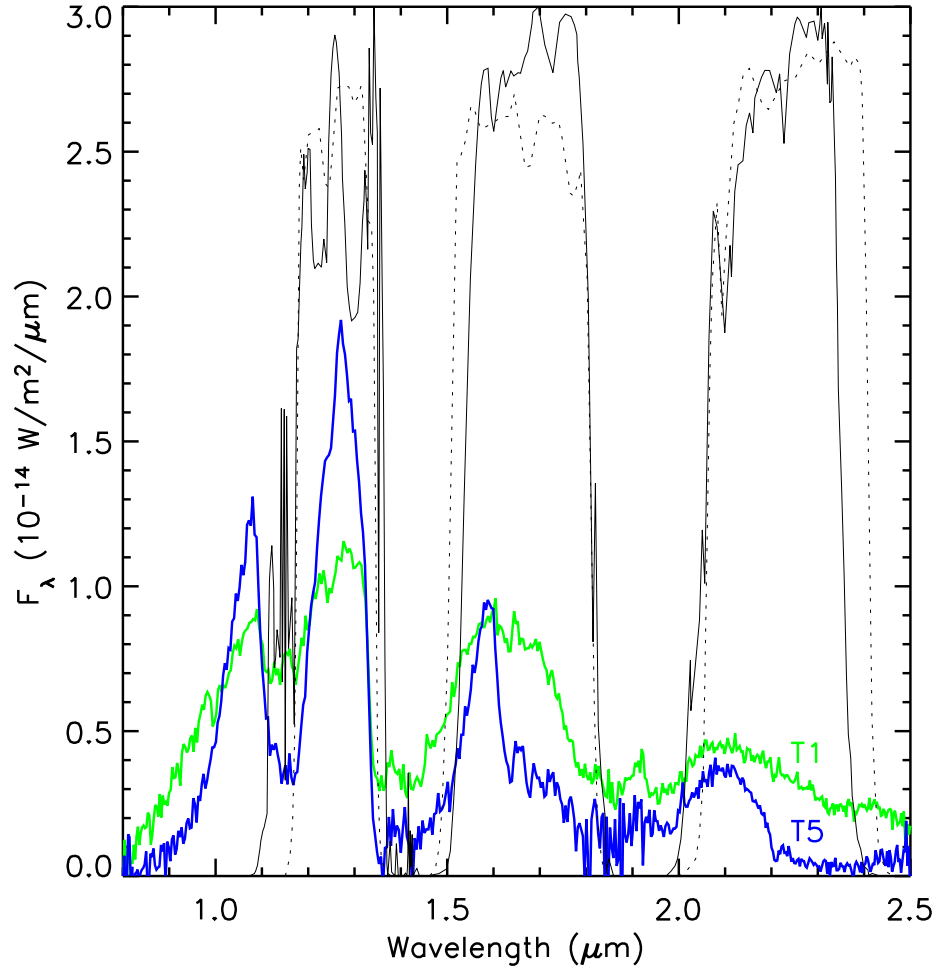


Fig. 7. Left: SDSS J205235.31-160929.8 (NIR T1; Chiu et al. 2006), shown in green, and 2M ASS J23312378-4718274 (NIR T5; Burgasser et al. 2004), shown in blue, scaled by the M KO magnitudes of the A and B components of 2M ASS 1404AB. The 2M ASS JH K_s (solid lines) and M KO JH K (dotted lines) transmission plus atmospheric profiles are overlaid.

TABLE 3
Coefficients of Polynomial Fits for L and T Dwarfs^a

R	c ₀	c ₁	c ₂	c ₃	c ₄	c ₅	c ₆	RM S
M _J ^b (mag)	11.817	1.255e-1	3.690e-2	1.663e-2	3.915e-3	2.595e-4	5.462e-6	0.29
M _H ^b (mag)	11.010	1.125e-1	3.032e-2	1.261e-2	2.970e-3	1.987e-4	4.218e-6	0.29
M _{K_s} ^b (mag)	10.521	7.369e-2	2.565e-2	1.299e-2	2.864e-3	1.911e-4	4.104e-6	0.33
BC _{K_s} ^{c,d} (mag)	3.221	2.371e-2	6.428e-3	1.631e-3	5.579e-5			0.16
T _{eff} ^d (K)	2319.920	108.094	1.950	3.101	6.414e-1	4.255e-2	9.084e-4	87

^a Polynomial fits to optical L dwarfs (classified on Kirkpatrick et al. 1999 scheme) and NIR T dwarfs (classified on Burgasser et al. 2006a scheme) with parallax measurements and not known to be binary (see x3.1 & x3.4 for a full description). Each function is defined as $R = \sum_{i=0}^n c_i (\text{SpT})^i$ and is valid for spectral types L0–T8, where 0 = L0, 10 = T0,

etc. These fits are shown graphically in Figs. 4 and 8.

^b Photometry is on the 2M ASS system.

^c Photometry is on the M KO system.

^d Data are from Golimowski et al. (2004) and references therein.

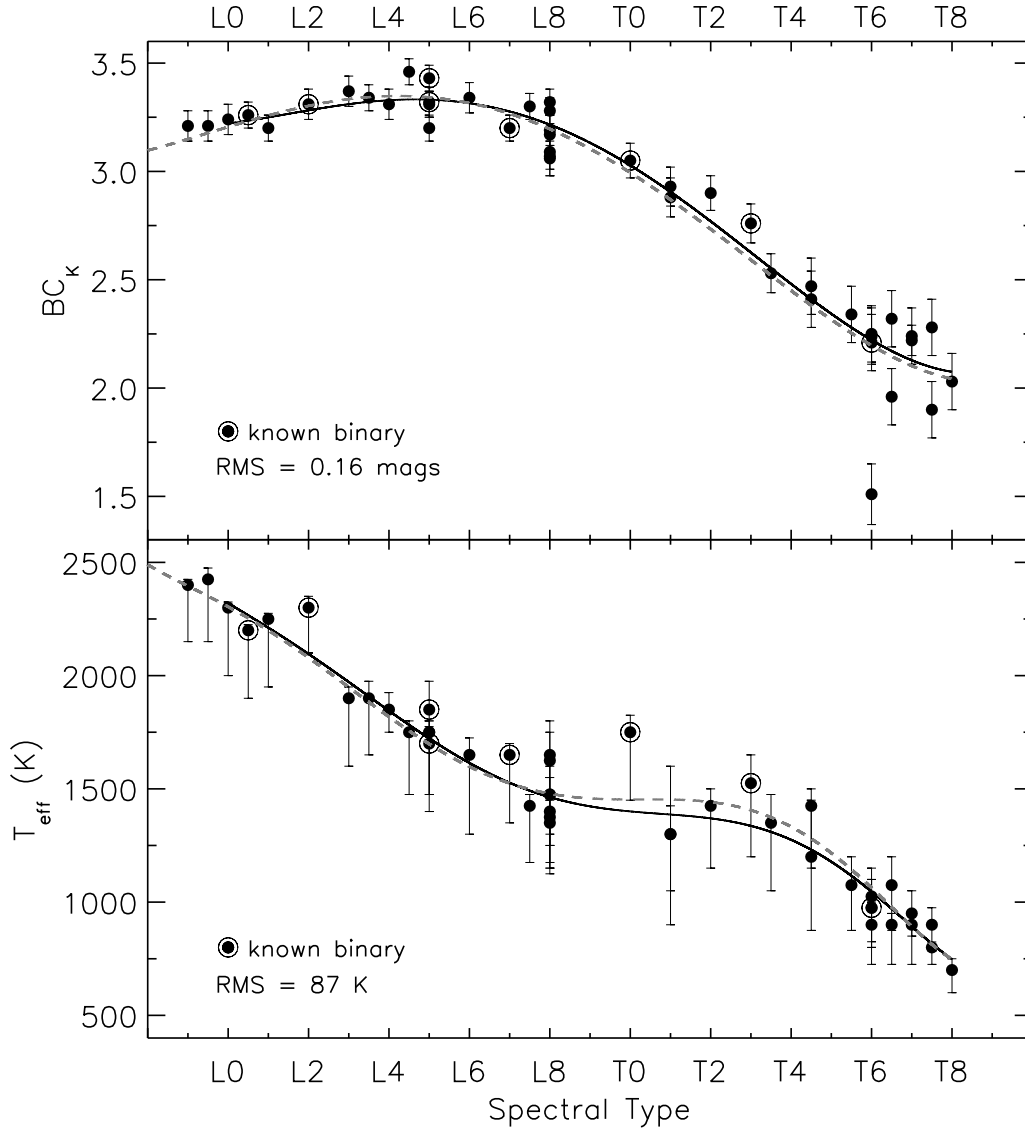


Fig. 8. | Polynomial fits (solid lines) to M 9{T8 objects with BC_K measurements and T_{eff} estimates (from Golimowski et al. 2004 and references therein), excluding known binaries. The relations are fourth- and sixth-degree polynomial fits for BC_K and T_{eff} , respectively, with the coefficients listed in Table 3. The plotted values used in the T_{eff} relation are for an age of 3 Gyr, and the error bars represent an age range of 0.1 { 10 Gyr (younger ages are cooler and older ages are hotter). The BC_K -SpT relation is weighted by the errors while the T_{eff} -SpT relation is unweighted. The large outlier seen in the BC_K plot and included in the fit is the T 6 dwarf 2MASS J0937347+ 293142, which is thought to be unusually blue due to high surface gravity/low-metallicity. Shown for comparison are the polynomial fits (dashed lines) from Golimowski et al. (2004).

TABLE 4
K-band Differences Between 2MASS and MKO by Spectral Type: L6.0{T2.0

Quantity	L6	L7	L8	L9	T0	T1	T2	AVG
2MASS K_s - MKO K	0.03	0.01	0.02	0.02	0.01	0.01	0.02	0.01
Number of Objects ^a	4	1	2	2	1	7	8	25

^a The number of objects available per spectral type class, where a class also includes a half-subtype - i.e., L6.0 and L6.5. Note that the T 2 spectral class only includes T 2.0 objects and no T 2.5 objects.

TABLE 5
Properties of the Components of the 2M ASS 1404AB System

Property	2M ASS 1404A		2M ASS 1404B	
M KO J (mags)	16.46	0.12	15.93	0.09
M KO H (mags)	15.56	0.09	16.04	0.10
M KO K (mags)	14.86	0.11	16.06	0.19
2M ASS J (mags)	16.65	0.12	16.20	0.09
2M ASS H (mags)	15.51	0.09	16.00	0.10
2M ASS K _s (mags)	14.83	0.11	15.96	0.19
M KO J H (mags)	0.90	0.15	0.11	0.13
M KO H K (mags)	0.70	0.14	0.02	0.21
M KO J K (mags)	1.60	0.16	0.13	0.21
2M ASS J H (mags)	1.14	0.15	0.20	0.13
2M ASS H K _s (mags)	0.68	0.14	0.04	0.21
2M ASS J K _s (mags)	1.82	0.16	0.24	0.21
Est: N IR SpT ^a	T 1	1	T 5	1
Est: T _{eff} (K) ^b	1390	90	1180	90
M _{bol} (mags)	15.96	0.19	16.59	0.25

^a Component N IR spectral types are derived in x3.2.

^b Based on the T_{eff} vs. SpT relation defined in Table 3, using the component spectral types listed and assuming an age of 3 Gyr.